Journal of Pathology
J Pathol 2003; **201**: 99–108.
Published online 1 July 2003 in Wiley InterScience (www.interscience.wiley.com). **DOI:** 10.1002/path.1421

Original Paper

Applications of Fourier transform infrared microspectroscopy in studies of benign prostate and prostate cancer. A pilot study

E Gazi,[1] J Dwyer,[1]* P Gardner,[1] A Ghanbari-Siahkali,[1] AP Wade,[1] J Miyan,[2] NP Lockyer,[1] JC Vickerman,[1] NW Clarke,[3] JH Shanks,[4] LJ Scott,[3] CA Hart[3] and M Brown[3]

[1]*Department of Chemistry, UMIST, PO Box 88, Manchester M60 1QD, UK*
[2]*Department of Biomolecular Sciences, UMIST, PO Box 88, Manchester M60 1QD, UK*
[3]*Genito-Urinary Cancer Research Group, Cancer Research UK, Paterson Institute, Christie Hospital NHS Trust, Manchester M20 4BX, UK*
[4]*Christie Hospital NHS Trust, Histopathology Department, Manchester M20 4BX, UK*

**Correspondence to: Professor J Dwyer, Department of Chemistry, UMIST, PO Box 88, Manchester M60 1QD, UK. E-mail: J.Dwyer@umist.ac.uk*

Received: 18 November 2002
Revised: 24 January 2003
Accepted: 28 March 2003

Abstract

Fourier transform infrared (FTIR) microspectroscopy has been applied to a study of prostate cancer cell lines derived from different metastatic sites and to tissue from benign prostate and Gleason-graded malignant prostate tissue. Paraffin-embedded tissue samples were analysed by FTIR, after mounting onto a BaF_2 plate and subsequent removal of wax using Citroclear followed by acetone. Cell lines were analysed as aliquots of cell suspension held between two BaF_2 plates. It was found that the ratio of peak areas at 1030 and 1080 cm^{-1}, corresponding to the glycogen and phosphate vibrations respectively, suggests a potential method for the differentiation of benign from malignant cells. The use of this ratio in association with FTIR spectral imaging provides a basis for estimating areas of malignant tissue within defined regions of a specimen. Initial chemometric treatment of FTIR spectra, using the linear discriminant algorithm, demonstrates a promising method for the classification of benign and malignant tissue and the separation of Gleason-graded CaP spectra. Using the principle component analysis, this study has achieved for the first time the separation of FTIR spectra of prostate cancer cell lines derived from different metastatic sites.

Keywords: prostate cancer; benign prostatic hyperplasia; cell lines; FTIR microspectroscopy; multivariate analysis

Introduction

Currently, within the UK, prostate cancer is the second most common cause of cancer-related death in males [1].

Early diagnosis of prostate cancer is a prerequisite for a good prognosis. The initial stage in the diagnosis of prostate cancer usually involves a physical examination and measurement of the concentration of prostate-specific antigen (PSA) in blood serum. However, PSA levels can be influenced by factors other than the presence of prostate cancer, which complicates diagnosis. Recently, it has been suggested that elevated levels of four peptides based on the deglycosylation of membrane-bound proteins of prostate cancer cells and subsequent antibody formation can assist in diagnosis [2].

Confirmation of the initial diagnosis involves a biopsy followed by grading using the method developed by Gleason [3]. Whilst such a grading system, in combination with clinical variables such as serum PSA and clinical stage, can predict the likelihood of cancer progression in populations, it cannot by itself predict the likelihood of metastasis in individuals, so that patients with the same Gleason grade can have very different mortality risks. A study by Lattouf *et al* [4] of 390 patients has shown that Gleason scoring by up to 15 pathologists resulted in 38.2% of tumours being undergraded and 32.6% overgraded. Identical Gleason grades by the pathologists were assigned to 29.2% of tumours, which indicates a limitation in its use in clinical decision-making.

Some general indications of prognosis can be provided, for example by reference to Partin tables [5] or, in the case of clinically localized cancer, by the use of a pre-operative nomogram, which has been reported to provide a reasonably accurate estimate of the effectiveness of surgery during the 5 years following the operation [6]. The current position with regard to the diagnosis and staging of prostate cancer has been reviewed by Narain *et al* [7].

Because of difficulties associated with predicting prognosis, there is considerable interest in developing procedures to identify the more aggressive cancers, either by elucidating the biochemical features of metastases or by seeking chemical markers to identify changes in the underlying biochemistry associated

with the development and progression of malignancy. One example of the former approach [8] uses Matrigel invasion chamber assays to demonstrate the invasive ability of malignant versus non-malignant prostate epithelial cells in response to bone marrow endothelial cells and suggests that this may be a critical step in the formation of metastases. In a similar vein, it has been reported that the ratio of cathepsin B (which helps cancer cells to invade surrounding healthy tissue) to stefan A (which blocks the action of cathepsin A) might provide an indication of the mechanisms of metastasis [9].

Currently, there is considerable interest in the evolution of imaging techniques [10] and in the development of spectroscopic analytical techniques, which can provide the biochemical signatures and processes associated with the generation and progression of malignancy. The application of vibrational spectroscopy, infrared (IR) and Raman, is much to the forefront in current research focusing on the development of practical diagnostic and/or prognostic tools. A recent review provides a good introduction to the application of infrared spectroscopy to the study of biological tissue [11]. IR spectra are representative of the chemical composition of the sample, so that changes in biochemistry can be monitored. In principle, FTIR analysis provides an opportunity to detect biochemical changes in addition to the architectural changes, which form the basis for Gleason grading.

FTIR microspectroscopy permits the rapid collection of spectra obtained from small well-defined spatial regions, of around $7 \times 7\ \mu m^2$, which can be scanned to provide a 'biochemical map' of a tissue specimen. Moreover, because IR radiation is a low-energy process, the imaging of any sample can be replicated numerous times to reduce intra/inter-specimen variability. Also, because the FTIR equipment is relatively inexpensive, this technique could have a role alongside conventional methods for grading prostate cancer tissue. However, because of the large number of data points acquired in FTIR spectra, together with the fact that the biochemical changes being monitored can be quite subtle, chemometric methods are helpful in identifying biochemical variance [12].

This pilot study represents a preliminary assessment of the role of FTIR spectroscopy in the comparison of epithelial cells from normal glands, benign prostatic hyperplasia (BPH), Gleason-graded prostate cancer tissue, and prostate cancer cell lines derived from different metastatic sites.

Materials and methods

Primary tissue collection for culture

All samples were obtained with informed consent from males undergoing treatment for urinary outflow obstructive symptoms by transurethral resection in which there was benign prostatic hyperplasia (BPH) or prostate adenocarcinoma (CaP). Three samples of CaP (EPC1, EPC2, and EPC3) and two samples of BPH (EPC4 and EPC5) were examined using FTIR microspectroscopy. Prostate epithelial cells were isolated from these samples by collagenase digestion followed by differential centrifugation, as described by Lang *et al* [13]. Epithelial cells were grown in flasks in Keratinocyte-SFM and used at passage 1. The culture technique outlined here is comparable to the procedure utilized for the cell lines, described below, and is used in preference to primary cells derived directly by post-collagenase and trypsin treatment of prostate chips. Thus, a direct spectroscopic comparison of the data obtained from primary tissue culture and cell lines is valid.

Cell lines

Non-malignant PNT2-C2 (normal prostate epithelial cells transfected with the genome of SV40 virus to express the large T antigen) [14] and DU 145 (derived from brain metastasis) [15] were cultured in RPMI 1640, 10% fetal calf serum (FCS), and 2 mM L-glutamine. PC-3 (derived from bone metastasis) was cultured in Ham's F12, 7% FCS, and 2 mM L-glutamine [16]. Cultures were grown at 37 °C in a humidified atmosphere of 5% CO_2 in air. When confluent, primary prostate epithelial cells or cell lines were trypsinized from the flask using 0.5% trypsin/EDTA solution and washed twice in phosphate-buffered saline (PBS). All reagents were purchased from Sigma-Aldridge, Poole, UK. All tissue culture media were obtained from Invitrogen, Paisley, UK, with the exception of Ham's F12 media (PAA Laboratories, Austria). FCS was supplied by Labtech International Ltd, Uckfield, Sussex, UK. Collagenase type 1 and trypsin were supplied by Lorne Laboratories Ltd, Twyford, UK.

Cell preparation for FTIR

All cells were stored in PBS and transported on ice. Cell suspensions were analysed by smearing onto a BaF_2 plate, after which another BaF_2 plate was placed above. This 'sandwich' method allowed for the minimal redistribution of cellular components caused by the evaporation of the PBS during spectrum acquisition.

Primary tissue preparation and sampling for FTIR

Archived CaP and BPH tissue biopsy specimens were obtained as paraffin wax-embedded blocks. These were sectioned at 10 μm using a Leica RM2155 Microtome and mounted onto BaF_2 plates (Linkam Scientific Ltd). The sections were then washed with Citroclear for 7 min to remove the paraffin wax and washed with cold (4 °C) acetone and then air-dried under ambient conditions before FTIR analysis.

Targeted spectra of benign and malignant prostate epithelial cells within the tissue matrix involved the collection of serial sections, from the specimen, one of which was mounted onto BaF_2 with the adjacent section mounted onto a glass slide and stained using haematoxylin and eosin (H&E) (Figure 1). It was then possible to use the luminal areas identified from the H&E section as landmarks that allowed for the positioning of the IR beam on the complementary section mounted onto the BaF_2 plate. In the present study, areas for analysis and Gleason grades were assigned by an experienced histopathologist (JHS).

Microspectroscopy and spectral imaging

FTIR spectra of all extracted cell suspensions from primary tissue culture, cell lines, and epithelial cells of BPH and Gleason-graded CaP primary prostate tissue were collected in transmission mode using a Nicolet Magna system 550 spectrometer equipped with a liquid nitrogen-cooled MCT/A detector and a KBr beam splitter. The spectrometer is attached to a microscope equipped with a television camera in order to view optical images of the sampling area and a programmable computerized x/y stage. The size of the lower aperture (confocal arrangement) is set so that it matches the projected image of the upper aperture. Where spectra were taken from benign prostate showing basal cell hyperplasia and CaP tissue, an aperture size of $60 \times 60\ \mu m^2$ was used. Spectra acquired from normal epithelial regions were taken with an aperture size of $48 \times 60\ \mu m^2$. Spectra taken from cell suspensions used an aperture size of $60 \times 78\ \mu m^2$.

FTIR spectra represent an average of 512 scans (tissue specimens) and 1024 scans (cell suspensions) in the wavenumber range 750–4000 cm^{-1}, with a resolution of 4 cm^{-1}. Background scans were obtained from a region of no sample and ratioed against the sample spectrum.

FTIR spectral imaging of primary prostate tissue was carried out in transmission mode using a Bio-Rad FTS 6000 spectrometer equipped with a liquid nitrogen-cooled 64×64 focal plane array detector (spatial resolution $6.5 \times 6.5\ \mu m^2$). Each spectrum was recorded with 513 co-added scans at 16 cm^{-1} resolution.

Data processing

Data processing immediately after spectrum acquisition was carried out using OMNIC v.5.1a software, which included the Atlus video capturing program. The Microcal Origin v.4.1 program was used for further processing and performed baseline correction (rubber band algorithm) and normalization of the spectra relative to the amide I peak (~1650 cm^{-1}). Normalized spectra were used to correct for differences in the path length of the IR beam and the number of cells analysed within the chosen aperture size.

Origin also allowed for the deconvolution of specific bands. The aim of this operation is to resolve the underlying and overlapping peaks present as a composite of a broad peak. The procedure mathematically enhances the resolution of the spectrum, using an iterative statistical curve fitting of symmetric Gaussian peaks to the straight, baseline-corrected spectra.

Principle component analysis (PCA) and linear discrimination analysis (LDA) were carried out using SPSS Release 11.0.0.

Results

FTIR spectra of benign and malignant prostate tissue

The average of four FTIR spectra acquired from epithelial cells of normal, BPH, and malignant prostate glands are presented in Figure 2. The typical sampling area from which these spectra were taken is represented by the blue box, (a)–(f). Within the sampling area, slight variations in the cell density may be measured, which are largely corrected by the normalization procedure applied to the spectra. It is evident that significant changes in the IR absorbance from normal to hyperplastic to neoplastic cells occur in the

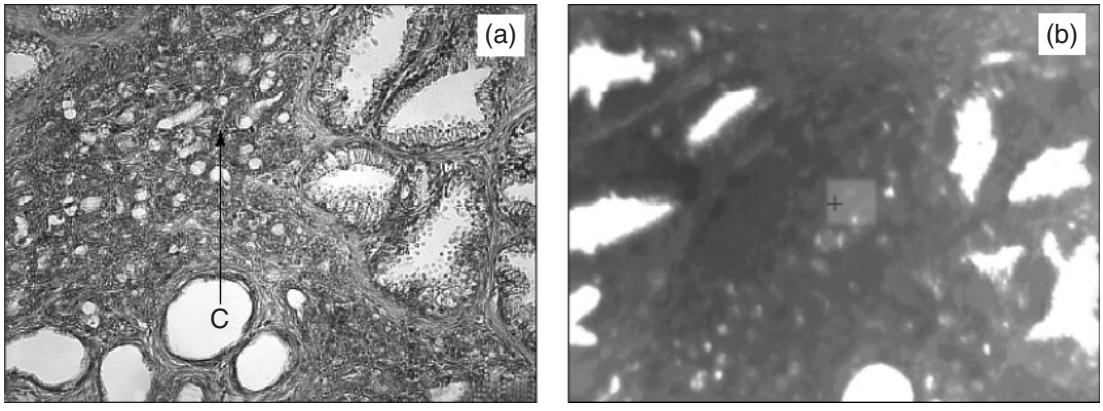

Figure 1. (a) Photomicrograph of an H&E-stained prostate tissue section. The arrow denotes the location of Gleason pattern 4 CaP (C). (b) Serial section of Citroclear-washed tissue on a BaF_2 plate. The square represents the infrared sampling area ($60 \times 60\ \mu m^2$)

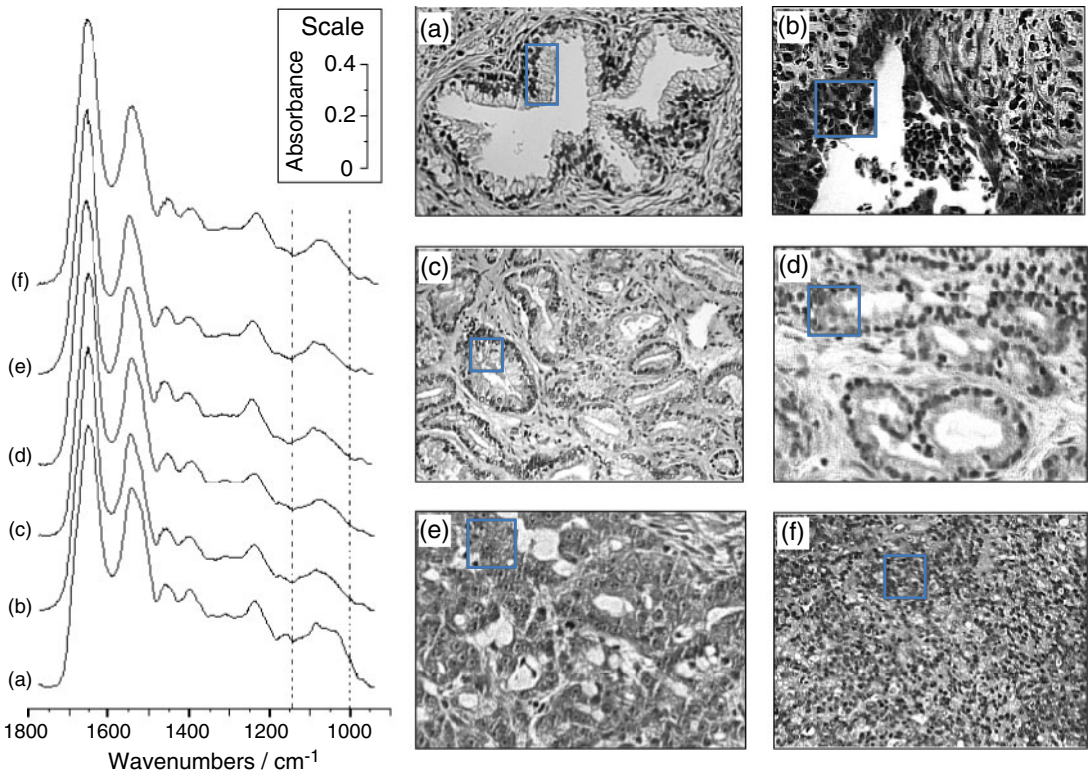

Figure 2. Average FTIR spectra in band region 1800–900 cm^{-1}, acquired from four epithelial cell locations of (a) normal prostate gland, (b) BPH, (c) Gleason pattern 2 CaP, (d) pattern 3 CaP, (e) pattern 4 CaP, and (f) pattern 5 CaP. The blue box in each photomicrograph represents a typical sampling area: (a) 48 × 60 μm; (b–f) 60 μm × 60 μm

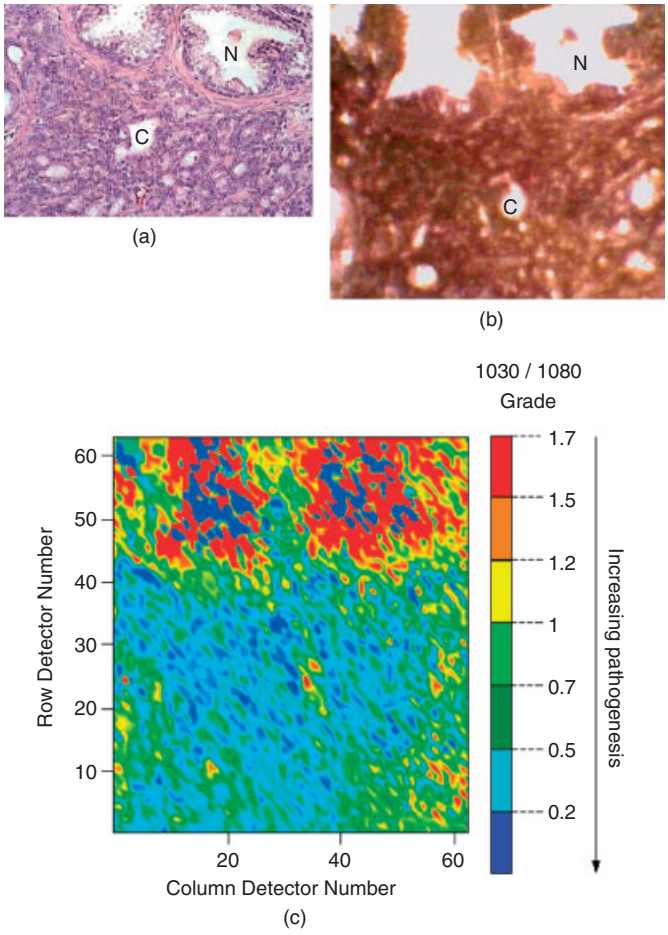

Figure 4. (a) Approximate imaging area on prostate tissue section. C = Gleason pattern 4 CaP; N = normal prostate gland. (b) FTIR imaging area of adjacent section of prostate tissue on a BaF_2 plate. (c) 1030 cm^{-1}/1080 cm^{-1} extracted spectral image

band region between 1000 and 1140 cm^{-1} (dotted vertical lines) and in the intensity ratio of peaks at 1650–1540 cm^{-1} arising from the protein amide I and II absorptions, respectively.

The Gleason score is derived from the sum of the primary and secondary Gleason patterns, each of the latter being between 1 and 5, with 1 representing the lowest grade (well differentiated) and 5 the highest (poorly differentiated). The Gleason score is thus between 2 and 10. Gleason patterns relate to the glandular architecture present in the tissue sections. A simplified description for each Gleason pattern is described below: a more detailed explanation of histopathological features is given in ref 3.

In Gleason pattern 2 (Figure 2c), relatively round malignant glands that are uniform in size and spacing are accepted. The glands are separated by fibrocollagenous matrix as the main component in the supporting connective tissue. In pattern 3 (Figure 2d), the malignant glands are less uniform in size and contour, with variable amounts of connective tissue between them. Pattern 4 (Figure 2e) demonstrates closer packing of glands, with loss of intervening connective tissue. Finally, pattern 5 (Figure 2f) refers to a tumour growing in undifferentiated sheets without gland formation. All malignant glands show loss of basal cells.

Within the spectrum of benign prostatic histology, there are various histological changes such as basal cell hyperplasia (BCH). In this study, we have analysed epithelial cells of BCH (Figure 2b).

Peak area ratio 1030 cm^{-1}/1080 cm^{-1} as a diagnostic marker

The peak area 1030 cm^{-1}/1080 cm^{-1} corresponds to the glycogen/phosphate ratio and is indicative of the metabolic turnover of the cell. This ratio has been used previously to differentiate neoplastic from non-neoplastic cells of different cancers [17,18]. To obtain the area values for these peaks, the region between 1000 and 1140 cm^{-1} for each spectrum was deconvoluted using four peaks (Figure 3). The functional group assignments have been made with respect to the locations of the centroids for each deconvoluted peak.

The 1030 cm^{-1}/1080 cm^{-1} area ratio values are presented in Table 1 for all cell suspensions and prostate tissues analysed.

Analysis of Table 1 shows that the decrease in ratio values obtained from cell suspensions of states C and CL may be correlated with increasing deviation from normal phenotype. More explicitly, on the basis of these data, we can assign an average ratio value of $\geq$0.6 as a benign condition and $\leq$0.4 as a malignant condition, thus providing a clear discriminative parameter that supports ratio values obtained from benign and malignant lung cells in another study [17]. Our analysis of prostate tissue produces ratio values that can also be used as potential diagnostic thresholds for distinguishing BPH (0.6–0.8) and adenocarcinoma ($\leq$0.5) from normal glandular epithelium ($\geq$1). The 1030 cm^{-1}/1080 cm^{-1} values between individual Gleason patterns do not show a correlation to increasing cancer aggressiveness.

The estimated standard deviation (SD) provides an indication of the heterogeneity in the sample matrix. To support this observed variance, a spectral image showing the distribution of the 1030 cm^{-1}/1080 cm^{-1} values across a tissue specimen was generated (Figure 4).

Figure 4a shows a region of Gleason pattern 4 carcinoma below an area of normal prostate glands and connective tissue. Using the colour intensity chart shown in Figure 4c, we can estimate approximate values for 1030 cm^{-1}/1080 cm^{-1}, to represent each colour in the spectral image. This may be carried out by assigning the highest intensity (red) as 100%, which corresponds to a mean ratio of 1.7 (excluding from analysis one outlier test value, see Table 1) for normal prostate epithelial cells. Accepting this scale, each colour can then be assigned a percentage of the total colour chart: 86% (orange), 71% (yellow), 57% (dark green), 43%

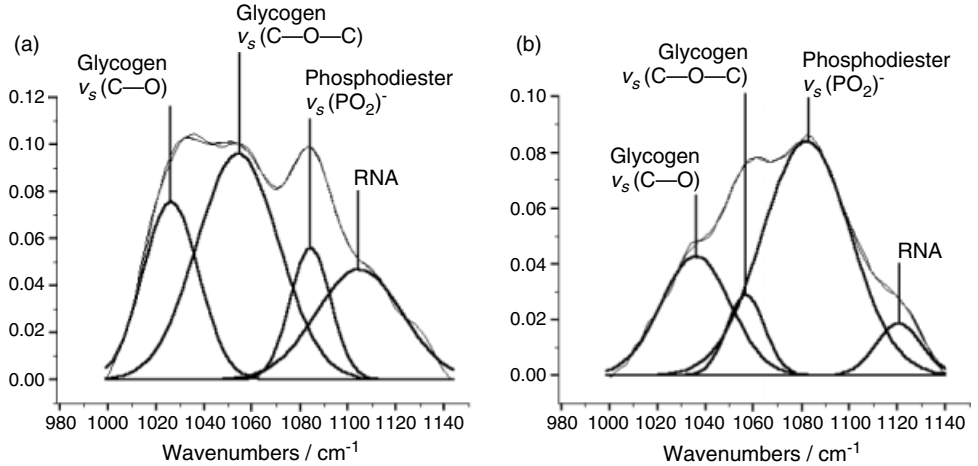

Figure 3. Deconvoluted spectra acquired from (a) normal prostate epithelial cells and (b) Gleason pattern 4 CaP cells in the band region 1000–1140 cm^{-1}

Table 1. Results from the area ratio of deconvoluted peaks 1030 cm^{-1}/1080 cm^{-1}

Sample No	Sample state	Pathogenic state	Spectral acquisition point	Gleason pattern	1030/1080 ratio		
					Tests	Mean	SD
1	T	Normal epithelial cells	1		1.65	2.37	1.32
			2		1.7		
			3		1.79		
			4		4.35		
2	C	EPC5 (BPH)	1		0.67	0.72	
			2		0.76		
3	C	EPC4 (BPH)	1		0.68	0.67	
			2		0.65		
4	T	BCH	1		0.7	0.67	0.13
			2		0.78		
			3		0.53		
1	T	CaP	1	3	0.42	0.44	0.08
			2		0.38		
			3		0.55		
			4		0.41		
1	T	CaP	1	4	0.4	0.37	0.03
			2		0.33		
			3		0.39		
					0.35		
5	T	CaP	1	5	0.24	0.29	0.07
			2		0.38		
			3		0.24		
			4		0.3		
6	C	DU 145	1		0.41	0.27	0.17
			2		0.33		
			3		0.08		
7	C	EPC2 (CaP)	1		0.38	0.26	
			2		0.14		
8	T	CaP	1	2	0.22	0.29	0.08
			2		0.25		
			3		0.41		
			4		0.29		
9	C	EPC3 (CaP)	1		0.17	0.17	
10	C	EPC1 (CaP)	1		0.14	0.15	
			2		0.16		
11	CL	PNT2-C2	1		0.04	0.13	
			2		0.21		
12	CL	PC3	1		0.07	0.06	
			2		0.04		

T represents spectra recorded from primary prostate tissue; C represents cell suspensions acquired from primary prostate tissue culture and CL represents cell lines. The standard deviation (SD) of ratio values for each of the spectral acquisition points is presented (see text for discussion).

(light green), 29% (turquoise), and 14% (blue). These values can then be used to estimate relative ratios for the 1030 cm^{-1}/1080 cm^{-1} peaks for the malignant region. Thus, a 1030 cm^{-1}/1080 cm^{-1} ratio value of 0.2–0.5 is obtained for turquoise regions and supports the mean 1030 cm^{-1}/1080 cm^{-1} value obtained for Gleason pattern 4 (0.37), presented in Table 1.

The spectral image in Figure 4c illustrates a clear distinction between regions of malignant tissue (turquoise/blue regions) and normal tissue (colour intensity, yellow and above). Upon closer examination, within each benign gland, we observe greater heterogeneity in its colour profile than is observed for malignant regions. This is discussed subsequently.

Data modelling using cluster analysis

PCA was successful in separating FTIR spectra acquired from cell suspensions of BPH, CaP, PNT2-C2, PC3, and DU 145 into clusters, within an orthogonally rotated space, as a function of a wavenumber–absorbance relationship (Figure 5a). The rotated component scores were then used as variables for LDA (Figure 5b). The PCA–LDA combined approach for spectra classification has been successfully applied to tissue spectra acquired by Raman spectroscopy [19,20]. However, our FTIR results showed no observable enhancement in the separation of clustered groups in the LDA plot from that obtained in the PCA plot.

It was also found that the PCA–LDA chemometric approach did not show separation of primary tissue spectra. However, FTIR spectral intensities for each tissue spectrum entered directly into LDA generated relatively well separated clusters corresponding to BCH and malignant glands of Gleason grades 2–5 (Figure 6).

Discussion

In this pilot study, we have demonstrated the potential use of FTIR to differentiate between benign and malignant prostate epithelial cells in tissue sections and cell lines derived from different metastatic sites. Additionally, although BPH is a common histological phenomenon, our preliminary data suggest the existence of chemical differences that can distinguish BPH from normal prostate glands.

Table 1 reveals an interesting result with regard to PNT2-C2, which is derived from normal prostate epithelial cells that have been transformed into an immortal cell line using the SV40 virus [14]. The 1030 cm^{-1}/1080 cm^{-1} value (0.13) for this cell line is within the range of values used to recognize malignancy in this study. The distribution of the

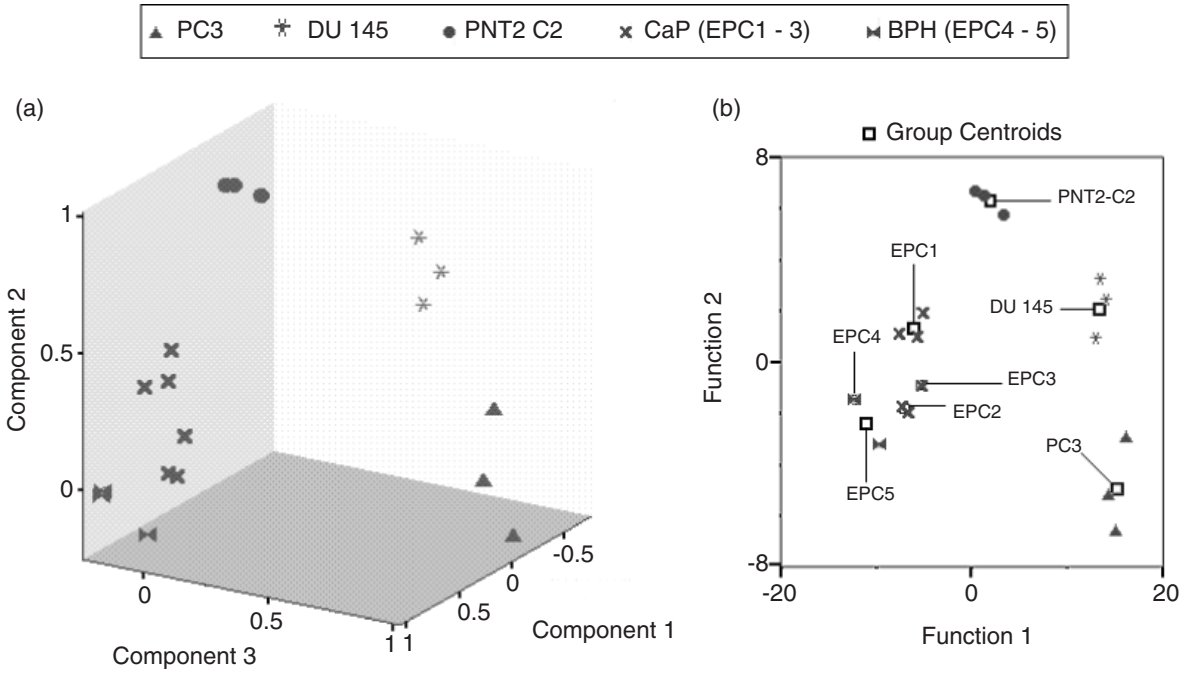

Figure 5. (a) Principle component plot in rotated space generated from PCA of FTIR spectra of cell lines and cell suspensions from primary tissue culture in band region 1483–940 cm^{-1}. (b) Combined-groups plot of linear discriminant function weights for principle component scores of cell lines and cell suspensions from primary prostate tissue culture

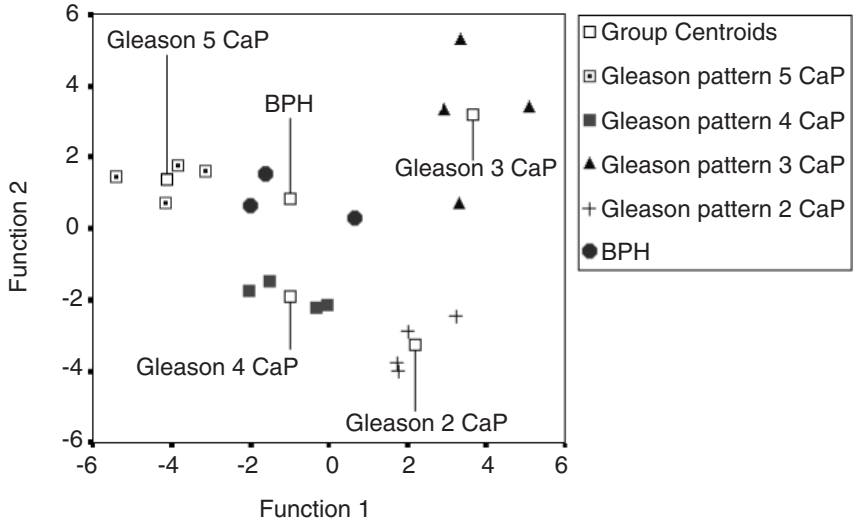

Figure 6. Combined-groups plot of linear discriminant function weights for FTIR spectra taken from prostate epithelial cells of BPH and malignant states in primary prostate tissue. Optimized separation of points was achieved using the FTIR spectral region 1481–1000 cm^{-1}

1030 cm^{-1}/1080 cm^{-1} values across the prostate tissue specimen shown in Figure 4c demonstrates the use of FTIR microspectroscopy as a diagnostic imaging tool. The homogeneous distribution of 1030 cm^{-1}/1080 cm^{-1} values observed within the malignant tissue provides supporting evidence for the close packing of malignant glands at Gleason pattern 4. Thus, variation in spectroscopic sampling from this region is influenced less by intervening connective tissue, basement membrane, basal cells or benign glands, which supports the low SD values obtained for pattern 4 CaP, presented in Table 1.

We interpret the values obtained for the 1030 cm^{-1}/1080 cm^{-1} ratio, shown in Table 1, as follows. The high glycogen content (1030 cm^{-1} peak) observed in normal prostate epithelial cell spectra (Figure 3a) may arise due to low metabolic activity. The majority of normal prostate cells analysed are terminally differentiated and have a low turnover/cycle rate. In contrast, the CaP spectrum in Figure 3b shows a lower glycogen content, as the majority of these cells are proceeding through their cell cycle and as a consequence, would be expected to exhibit a relatively higher metabolic activity. This is supported through FTIR studies by Takahashi *et al*, who observed a correlation between a decrease in glycogen content with increasing proliferation index of colorectal cancer cells [21]. They reported that cancer tissue having a high population of cells in the synthesis (S) and Gap_2-mitosis (G_2-M) phases exhibit lower glycogen levels than tissue with a high population of cells in the Gap_1 phase.

Glycogen stores have been reported to be used in CaP for cellular activities such as the increased *de novo* synthesis of lipids [22] or the generation of ATP molecules [23]. With respect to the latter, when a cell requires energy, glycogen is broken down through the process of glycolysis, generating pyruvate, which is then metabolized to form acetyl-CoA. This molecule fuels the citric acid cycle with the accompanying production of ATP molecules. The increased energy requirement by proliferating CaP cells has been reported to be a consequence of the zinc–citrate relationship in prostate malignancy by Costello and Franklin [23]. Zinc, which is present at higher levels in the prostate than in any other organ in the body, inhibits the enzyme m-aconitase present in the citric acid cycle and prevents the catalytic oxidation of citrate to isocitrate. However, in CaP, the zinc levels fall, which permits the m-aconitase-catalysed oxidation reaction to occur. This can result in the continuation of the citric acid cycle and the generation of ATP molecules, which would increase the need for the conversion of glycogen to pyruvate. These additional ATP molecules can be converted to ADP by specific protein kinase allowing for the phosphorylation of specific amino acid moieties (serine, threonine or tyrosine) expressed by oncoproteins [24]. Alternatively, ATP molecules can be utilized for the phosphorylation of membrane-bound, channel-ion proteins allowing for the subsequent entry of elemental ions needed for cell proliferation. The implications of intercellular ionic imbalances have previously been correlated to carcinogenesis [25–27].

PCA is a method of factor analysis which identifies underlying variables that explain the patterns of correlations within a set of observed variables (the spectral intensity at each wavenumber). Figure 5a shows the classification of pathogenic cell lines into clusters that are separated according to spectral variance, which correlates with biochemical variance. The rotated component scores for each spectrum were entered into the LDA algorithm. LDA attempts to find linear combinations of variables, for a given set of independent variables, that best separate groups of spectra. These combinations are termed discriminant functions. Function 1 separates the groups as far as possible. Function 2 is uncorrelated with function 1 and further separates the groups, the result of which allows for the maximum separation between groups and minimal separation within groups.

In Figure 5 we observe a large separation in cluster groups corresponding to cell lines PC3 and DU 145 from BPH and epithelial cells extracted from localized prostate cancer. We suggest that this separation may be due to specific biochemical features related to their invasive properties in Matrigel invasion assays. It has been reported that in Matrigel invasion studies, the PC3 [8] and DU 145 (unpublished observations, CH, NC, MB) cell lines exhibit high invasive properties when stimulated by bone marrow endothelial cells. We can correlate this invasiveness with the PCA–LDA plot in Figure 5, which shows a similar weighting upon function 1 of PC3 and DU 145 (14.8 and 16.8, respectively) and supports a biochemical relationship between these cell lines. The separation of the PNT2-C2 cluster from those of other pathogenic cells is due to transformation, which places this cell line, on the basis of the 1030 cm^{-1}/1080 cm^{-1} value, within the malignancy range (Table 1). However, it differs from the PC3 and DU 145 cell lines in that it shows no invasive properties in Matrigel studies [8]. This difference is also supported by the weighting value of 2.8 upon function 1 for PNT2-C2 in the LDA plot.

Additionally, the separation observed between DU 145 and PC3 suggests underlying biochemical differences between these types of cells. Overall, these initial results suggest promise for the identification of different types of metastatic cells.

The separation of clustered groups for spectra acquired from BPH and each Gleason-graded tissue by LDA is shown in Figure 6. It is important to note that FTIR spectra acquired from the BPH and graded prostate tissue are taken from epithelial cells only. Thus, the degree of tissue architecture differentiation, which is important in determining Gleason grade, is an indirect variable associated with the LDA algorithm. The direct variable entered into LDA is associated with spectroscopic differences derived from changes in cytological features such as the nucleus-to-cytoplasm

ratio, pleomorphism (variation in the size and shape of the cell), and biochemical composition.

A larger data set and appropriate statistical testing are necessary to construct a FTIR–LDA template incorporating suitable reference standards corresponding to each Gleason-graded CaP and BPH. Once this has been established, the algorithm can be evaluated in the classification of unknown spectra taken from tissue derived from prostate cancer patients, on the basis of proximity of the newly entered data to any one of the predefined cluster groups. This evaluation is currently being investigated with a view to establishing a standardized method in the grading of prostate cancer tissue.

In summary, imaging FTIR microspectroscopy represents a very fast, simple, and relatively inexpensive technique for the study of prostate cancer. The ratio of peak intensities at 1030 cm^{-1} and 1080 cm^{-1} is seen to provide information, which suggests a potential marker to distinguish between transformed normal cell lines and cell lines derived from various metastatic sites as well as cell suspensions of BPH and CaP. Additionally, the same criterion demonstrates a potential for the differentiation of normal and neoplastic prostate tissue. Moreover, the extent of malignant versus benign tissue within a sample can be estimated using IR imaging.

Preliminary data analysis using chemometric methods permits discrimination between cell lines, or between samples (or within samples) of primary tissue, based on the use of extensive regions of the IR spectra. Bio-spectroscopic information of the type outlined above could be readily incorporated into grading by histopathology, potentially assisting in diagnostic assessment in problematic cases. In addition, the optimization of chemometric procedures should result in an improved definition of malignancy and in a reduction in the variance identified by Lattouf and Saad [4].

A clearer understanding of the biochemical processes associated with the changes detected by imaging FTIR microspectroscopy will be developed from correlations of elemental ion concentrations and molecular fragments, currently being established using time-of-flight secondary ion mass spectrometry (ToF-SIMS).

Acknowledgements

We acknowledge the Engineering and Physical Sciences Research Council (EPSRC) for financial support (EG and APW) and Nicolet for additional support (to APW). We are grateful to Dr Roger Speak for use of FTIR equipment in Manchester University and Mr Gary Ashton and Miss Caron Abbey for the preparation of histological sections. We would like to dedicate this paper to the memory of Roy Nixon, who was both active and inspirational to the development of patient support groups and who first discussed the diagnosis of prostate cancer with one of us (JD).

References

1. Cancer Stats, Mortality — UK. June 2002, Cancer Research UK. http://www.cancerresearchuk.org/images/11632/cancerstats_mortality_2002.pdf [30 October 2002].
2. Seabury CA, Calenoff E, Ditlow C, *et al*. Evaluation of a new serum testing method for detection of prostate cancer. *J Urol* 2002; **168**: 93–99.
3. Gleason DF. Histologic grading and clinical staging of prostatic carcinoma. In *Urological Pathology — The Prostate*, Tannenbaum M (ed). Lee and Febiger: Philadelphia, 1977; 171–197.
4. Lattouf JB, Saad F. Gleason score on biopsy: is it reliable for predicting the final grade on pathology? *BJU Int* 2002; **90**: 694–699.
5. Partin AW, Walsh PC, Epstein JI, Pearson JD. Contemporary update of prostate cancer staging nomograms (Partin tables) for the new millennium. *Urology* 2001; **58**: 843–848.
6. Kattan MW. Radical radiation for localized prostate cancer: local persistence of disease results in a late wave of metastases. *J Clin Oncol* 2002; **20**: 3206–3212.
7. Narain V, Cher ML, Wood DP. Prostate cancer diagnosis, staging and survival. *Cancer Metastasis Rev* 2002; **21**: 17–22.
8. Scott LJ, Clarke NW, George NJR, Shanks JH, Testa NG, Land SH. Interactions of human prostatic epithelial cells with bone marrow endothelium: binding and invasion. *Br J Cancer* 2001; **84**: 1417–1423.
9. Sinha AA, Quast, Barry J, *et al*. Prediction of pelvic lymph node metastasis by the ratio of cathepsin B to stefin A in patients with prostate carcinoma. *Cancer* 2002; **94**: 3141–3149.
10. Benara DA. The future of cancer imaging. *Metastasis Rev* 2002; **21**: 45–78.
11. Diem M, Boydston-White S, Chiriboga L. Infrared spectroscopy of cells and tissues: shining light onto a novel subject. *Appl Spectrosc* 1999; **53**: 148A–161A.
12. Romeo M, Burden F, Quinn M, Wood B, McNaughton D. Infrared microspectroscopy and artificial neural networks in the diagnosis of cervical cancer. *Cell Mol Biol* 1998; **44**: 179–187.
13. Lang SH, Clarke NW, George NJ, Allen TD, Testa NG. Interaction of prostate epithelial cells from benign and malignant tumor tissue with bone-marrow stroma. *Prostate* 1998; **34**: 201–13.
14. Berthon P, Cussenot O, Hopwood L, Le Luc A, Maitland NJ. Functional expression of SV40 in normal human prostatic epithelial and fibroblastic cells: differentiation pattern of non-tumourigenic cell lines. *Int J Oncol* 1995; **6**: 333–343.
15. Mickey DD, Stone KR, Wunderli H, Mickey GH, Paulson DF. Characterization of a human prostate adenocarcinoma cell line (DU-145) as a monolayer culture and as a solid tumor in athymic mice. *Prog Clin Biol Res* 1980; **37**: 67–84.
16. Kaighn ME, Narayan KS, Ohnuki Y, Lechner JF, Jones LW. Establishment and characterization of a human prostatic carcinoma cell line (PC-3). *Invest Urol* 1979; **17**: 16–23.
17. Wang H-P, Wang H-C, Huang Y-J. Microscopic FTIR studies of lung cancer cells in pleural fluid. *Sci Total Environ* 1997; **204**: 283–287.
18. Ramesh J, Salman A, Hammody Z, *et al*. Applications of FTIR microscopy for the characterization of malignancy: H-ras transfected murine fibroblasts as an example. *J Biochem Biophys Methods* 2001; **50**: 33–42.
19. Stone N, Kendall C, Shepherd N, Crow P, Barr H. Near-infrared Raman spectroscopy for the classification of epithelial pre-cancers and cancers. *J Raman Spectrosc* 2002; **33**: 564–573.
20. Bakker Schut TC, Wolthuis R, Caspers PJ, Puppels G. Real-time tissue characterization on the basis of *in vivo* Raman spectra. *J Raman Spectrosc* 2002; **33**: 580–585.
21. Takahashi S, Satomi A, Yano K, *et al*. Estimations of glycogen levels in human colorectal cancer tissue: relationship with cell cycle and tumour outgrowth. *J Gastroenterol* 1999; **34**: 474–480.
22. Swinnen JV, Verhoeven G. Androgens and the control of lipid metabolism in human prostate cancer cells. *J Steroid Biochem Mol Biol* 1998; **65**: 191–198.

23. Costello LC, Franklin RB. Novel role of zinc in the regulation of prostate citrate metabolism and its implications in prostate cancer. *Prostate* 1998; **35**: 285–296.
24. Piris MA, Sanchez-Beato M, Villuendas R, Martinez JC. Oncogenes and tumour-suppressor genes. In *Cell Proliferation in Cancer: Regulatory Mechanisms of Neoplastic Cell Growth*, Lewis CE, Pusztai L, Yap E (eds). Oxford University Press: New York, 1996; 49.
25. Paluszkiewicz C, Kwiatek WM. Analysis of human cancer prostate tissues using FTIR microscopy and SRIXE techniques. *J Mol Struct* 2001; **565–566**: 329–334.
26. Kukus-Kubala A, Braziewicz J, Banas D, Majewska U, Gozdz S, Urbaniak A. Trace element load in cancer and normal lung tissue. *Nucl Instrum Methods Phys Res B* 1999; **150**: 193–199.
27. Huang Y-L, Sheu J-Y, Lin T-H. Association between oxidative stress and changes of trace elements in patients with breast cancer. *Clin Biochem* 1999; **32**: 131–136.

